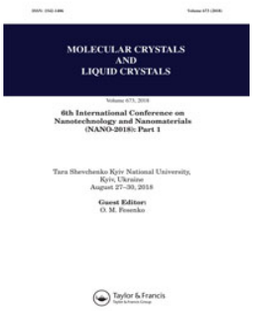

Molecular Crystals and Liquid Crystals

ISSN: 1542-1406 (Print) 1563-5287 (Online) Journal homepage: https://www.tandfonline.com/loi/gmcl20

Electronic and photonic properties of lateral heterostructures based on functionalized graphene depending on the degree of fluorination

R. Balabai, A. Solomenko & D. Kravtsova

To cite this article: R. Balabai, A. Solomenko & D. Kravtsova (2018) Electronic and photonic properties of lateral heterostructures based on functionalized graphene depending on the degree of fluorination, Molecular Crystals and Liquid Crystals, 673:1, 125-136, DOI: 10.1080/15421406.2019.1578502

To link to this article: https://doi.org/10.1080/15421406.2019.1578502

Published online: 19 Jun 2019.

MOLECULAR CRYSTALS AND LIQUID CRYSTALS
2018, VOL. 673, NO. 1, 125–136
https://doi.org/10.1080/15421406.2019.1578502

Taylor & Francis
Taylor & Francis Group

Electronic and photonic properties of lateral heterostructures based on functionalized graphene depending on the degree of fluorination

R. Balabai, A. Solomenko, and D. Kravtsova

Kryvyi Rih State Pedagogical University, 54 Gagarina Ave., Kryvyi Rih, 50086, Ukraine

ABSTRACT.
Within the framework of the methods of the electron density functional and the ab initio pseudopotential, the spatial distributions of the valence electron density, the distribution of electron states by energies in the valence and conduction bands, dielectric matrices and the macroscopic relative permeability of lateral heterostructures based on functionalized graphene as photonic crystals depending on the degree of fluorination were obtained.

KEYWORDS
lateral heterostructure; functionalized graphene; the electron density functional; ab initio pseudopotential; absorption spectrum; fluorination

Introduction

Lateral, in-plane heterostructures (HSs) in which one-dimensional junctions are created between the different materials are very interesting. These kinds of HSs open the possibility to obtain ultimately thin devices [1]. Using certain technological methods, by creating on the graphene plane some local adsorption parts of various chemical elements (functionalization), it is possible to organize lateral HSs on a common carbon base [2]. Such lateral HSs exhibit diode properties [3]. The periodic alternation parts of pure graphene (C) and functionalized graphene (namely graphane – CH) have different dielectric permittivity, which gives grounds to consider such structures as photonic crystals (PhCs) and to investigate their photonic properties [4].

The authors [5] reported a study two-dimensional graphene-based photonic crystal formed by a periodic array of the homogeneous dielectric cylinders etched in the alternating graphene and dielectric layers and its inverse counterpart. It was proved that the band structure and localization of photonic modes can be modified by two ways: by engineering the crystal lattice, choosing the dielectric and the radius of the cylinder during the manufacture and via doping of graphene layers. During the manufacture the band gap as well as the localized modes can be controlled by the type and thickness of the dielectric that separates the graphene layers, as well as by the filling factor and lattice constant.

The transmission properties of a one-dimensional photonic crystal containing graphene mono-layers were studied using the transfer matrix method in work [6]. It was shown that the structure can be used as a polarization-selective nonreciprocal device which discriminates between the two circularly polarized waves with different

CONTACT R. Balabai balabai@i.ua; A. Solomenko solomenko.anastasiia@gmail.com

handedness impinging in the same direction. This structure may be utilized in designing optical isolators for the circularly polarized waves due to the gyrotropic behavior of the graphene mono-layers under the perpendicularly applied external magnetic field.

It was reported [7] that fluorinated graphene sheets (FGSs) exhibit full-color emission when excited by near ultraviolet (NUV) rays, suggesting its potential applications in luminescence devices, such as NUV-pumped FGS-based flexible light-emitting diodes. It was reported that graphene fluoride colloids exhibit high third-order nonlinear optical response, suggesting their potential application in photonic and opto-electronic devices [8].

Interesting graphene-based plasmonic PhCs with ultra-small size were proposed in work [9]. Photonic band gaps were found in both 1D and 2D PhCs. The proposed graphene based PhC structure might find broad applications in the future high density plasmonic integrated circuit technique.

Recently, a new 2D counterpart of graphane, namely hydrogenated fluorographene (CFH), was obtained by benign wet chemical synthesis. The authors emphasized its significant nonlinear optical properties. They revealed the importance of the nature of the functional group and the degree of functionalization on the nonlinear optical properties of graphenes [10, 11].

Our research was to study electronic and photonic properties of the lateral HSs based on functionalized graphene as PhCs depending on the degree of fluorination. The valence electrons density spatial distribution, the densities of electron states, the band gaps, the charges on parts of HSs (PhCs), the dielectric matrices, and the macroscopic permittivities were obtained in the framework of the electronic density functional and ab initio pseudopotential based on own program code [12].

Methods of research

The basic states of the electron-nucleus systems were detected by means of the self-consistent solution of the Kohn-Sham equations. Electronic variables only were determined with the atomic cores fixed. Following Kohn-Sham [13, 14], electronic density was written down in terms of occupied orthonormal one-particle wave functions:

$$n(\vec{r}) = \sum_i |\psi_i(\vec{r})|^2. \tag{1}$$

The point on the surface of potential energy in the Born-Oppenheimer approximation was determined as a minimum energy functional with regard to the wave functions:

$$E\left[\{\psi_i\},\{R_j\},\{\alpha_\nu\}\right] = \sum_i \int_\Omega d^3 r \psi_i^*(\vec{r}) \left[-\frac{\hbar^2}{2m}\nabla^2\right]\psi_i(\vec{r}) + U\left[\left\{n(\vec{r})\right\},\{R_j\},\{\alpha_\nu\}\right], \tag{2}$$

where $\{R_j\}$ are coordinates of atomic cores; $\{\alpha_\nu\}$ are any external influences on the system.

In the generally accepted formulation, minimization of the energy functional (2) with respect to one-particle orbitals with additional orthonormal constraint on the one-particle orbitals results in Kohn-Sham one-particle equations [14]:

$$\left\{-\frac{\hbar^2}{2m}\nabla^2+\frac{\partial U}{\partial n(\vec{r})}\right\}\psi_i(\vec{r})=\varepsilon_i\psi_i(\vec{r}). \tag{3}$$

In the solution of these equations, the pseudopotential formalism was used, according to which a solid is considered as a set of valence electrons and the ion cores. In the pseudopotential approximation, the operator of the pseudopotential V_{PS}, which describes the interaction of valence electrons with the core, is small, and the corresponding pseudo-wavefunction is smooth. Pseudopotential are required to correctly represent the long range interactions of the core and to produce pseudo-wavefunction solutions that approach the full wavefunction outside a core radius r_c. In addition it is desired that a pseudopotential is transferable, this means that one and the same pseudopotential can be used in calculations of different chemical environment resulting in calculations with comparable accuracy. For example, Bachelet, Hamann and Schlüter proposed an analytic fit to the pseudopotentials [15, 16]. This ab initio pseudopotential is used by us.

The full crystalline potential is constructed as the sum of ion pseudopotentials that are not overlapping and associated with ions (nucleus + core electrons), located at the $\vec{R}_S$ positions that are periodically repeated for crystals:

$$V_{cryst}(\vec{r})\rightarrow V_{PS}(\vec{r})=\sum_{\vec{p}}\sum_{S}\hat{V}_S^{PS}\left(\vec{r}-\vec{p}-\vec{R}_S\right). \tag{4}$$

For nonperiodic systems, such as a thin film or a cluster the problem of lack of periodicity is circumvented by use of the supercell method [17, 18]. Namely, the cluster is periodically repeated but the distance between each cluster and its periodic images is so large that their interaction is negligible. The ubiquitous periodicity of the crystal (or artificial) lattice produces a periodic potential and thus imposes the same periodicity on the density (implying Bloch's Theorem). The Kohn-Sham potential of a periodic system exhibits the same periodicity as the direct lattice and the Kohn-Sham orbitals can be written in Bloch form:

$$\psi(\vec{r})=\psi_i\left(\vec{r},\vec{k}\right)=\exp\left(i\vec{k}\cdot\vec{r}\right)u_i\left(\vec{r},\vec{k}\right), \tag{5}$$

where $\vec{k}$ is a vector in the first Brillouin zone. The functions $u_i(\vec{r},\vec{k})$ have the periodicity of the direct lattice. The index i runs over all states. The periodic functions are expanded in the plane wave basis. This heavily suggests to use plane waves as the generic basis set in order to expand the periodic part of the orbitals. Since plane waves form a complete and orthonormal set of functions, they can be used to expand orbitals according to:

$$\psi_j\left(\vec{k},\vec{r}\right)=\frac{1}{\sqrt{N_0}\sqrt{\Omega}}\sum_{\vec{G}}b_j\left(\vec{k}+\vec{G}\right)\exp\left(i\left(\vec{k}+\vec{G}\right)\vec{r}\right), \tag{6}$$

where $\vec{G}$ is the vector in the reciprocal space, Ω is the volume of the elemental cells which consists of a periodic crystal or an artificial superlattice when reproducing nonperiodic objects.

The equation (6) after the Fourier transform to the reciprocal space has the form:

$$\sum_{\vec{G}}\left[\left\{\frac{\hbar^2}{2m}\left(\vec{k}+\vec{G}\right)^2-\varepsilon_j\right\}\delta_{\vec{G},\vec{G}'}+V_{KS}\left(\vec{k}+\vec{G},\vec{k}+\vec{G}'\right)\right]b_j\left(\vec{k}+\vec{G}\right)=0, \tag{7}$$

where V_{KS} is the Kohn-Sham potential:

$$V_{KS}\left(\vec{k}+\vec{G},\vec{k}+\vec{G}'\right)=V_{PS}\left(\vec{k}+\vec{G},\vec{k}+\vec{G}'\right)+V_H\left(\vec{G}'-\vec{G}\right)+V_{XC}\left(\vec{G}'-\vec{G}\right), \tag{8}$$

where V_{XC} is the exchange and correlation potential. To calculate its we used Ceperley-Alder's approximation that has been parameterized by Perdew and Zunger.

In the general case, the expressions describing the potentials of interactions are complex. The use of the atomic bases containing the inversion operation in the point symmetry group leads to the fact that the Fourier-components in the expansion of all expressions are real.

The main value in the formalism of the functional of the electron density is the charge density. It is estimated from a self-consistent solution of equations (7) which should be performed at all points of the non-reduced section of the Brillouin zone:

$$\rho(\vec{G})=\frac{2}{N_T}\sum_k\sum_j\sum_{\alpha\in T}\sum_{\vec{G}'}b_j^*\left(\vec{k}+\vec{G}'+\alpha\vec{G}\right)b_j\left(\vec{k}+\vec{G}'\right), \tag{9}$$

where the index j runs over all occupied states, $\vec{k}$ is a vector in the first Brillouin zone, N_T is the number of the operators α in the point group T of the atomic basis and the factor 2 takes into account the spin degeneracy.

Estimated effort can be reduced if there is the integral over the Brillouin zone to approximate by summing over a special point of the Brillouin zone. It is possible to replace with satisfactory precision the summation by the finite number of special points to one point in the Brillouin zone. It is possible to restrict only the Γ-point in the Brillouin zone, especially as it relates to the artificial periodic systems.

Distribution of electrons along the energy zones for Γ-state of the investigated structures was found by means of numerical calculation of derivative $\lim_{\Delta E\to 0}\Delta N/\Delta E$ (where ΔN is a number of the allowed states for the ΔE interval of energy). The one-particle energy spectrum was obtained from calculation of the eigenvalues of the Kohn-Sham matrix. In accordance with ideology of the electronic density functional, the occupied states at absolute zero temperature were defined. It allowed to define position of the last occupied state, their number being half the number of electrons (due to ignoring the spin of the electron), and position of the first free states.

The solid state linear response to perturbation is described by a dielectric matrix. In our computational experiments, the static dielectric matrix was estimated from the electronic structure of the ground state of the crystalline system (occupied and unoccupied states). The dielectric matrix $\in^{-1}_{\vec{G},\vec{G}'}(\vec{q},\vec{\omega})$ was calculated in reciprocal space and depended on the wave vector $\vec{q}$ and the oscillation frequency of the electric field of the perturbing electromagnetic wave $\vec{\omega}$ ($\vec{G}$ – reciprocal lattice vectors). Non-diagonal elements of the matrix $\in^{-1}_{\vec{G},\vec{G}'}$ determine the local effects of the field. The macroscopic dielectric function was [19]:

$$\in_M\left(\vec{q}+\vec{G}\right)=\frac{1}{\in_{00}^{-1}(\vec{q})} \tag{10}$$

To get the elements of the matrix, the equation in the reciprocal space was solved:

$$\in_{\vec{G},\vec{G}\prime}^{-1}(\vec{q})=\delta_{\vec{G}\vec{G}'}+\frac{4\pi e^2}{|\vec{q}+\vec{G}|^2}\chi_{\vec{G}\vec{G}'}(\vec{q}), \tag{11}$$

where polarization was defined as

$$\chi_{\vec{G}\vec{G}'}(\vec{q})=\sum_{\vec{G}''}A^{-1}_{\vec{G}\vec{G}\prime\prime}(\vec{q})\chi^0_{\vec{G}\prime\prime\vec{G}\prime}(\vec{q}), \tag{12}$$

$$A_{\vec{G}\vec{G}'}(\vec{q})=\delta_{\vec{G}\vec{G}'}-\chi^0_{GG\prime}(\vec{q})\frac{4\pi e^2}{|\vec{q}+\vec{G}\prime|^2}-\sum_{\vec{G}''}\chi^0_{\vec{G}\vec{G}\prime}(\vec{q})K_{XC}\left(\vec{G}''-\vec{G}'\right), \tag{13}$$

$$\chi^0_{\vec{G}\vec{G}\prime}(\vec{q})=\frac{4}{\Omega}\sum_{c,v,\vec{k}}\frac{\langle v,\vec{k}|e^{-i\left(\vec{q}+\vec{G}\right)\vec{r}}|c,\vec{k}+\vec{q}\rangle\langle c,\vec{k}+\vec{q}|e^{i\left(\vec{q}+\vec{G}\prime\right)\vec{r}\prime}|v,\vec{k}\rangle}{\varepsilon_{v,\vec{k}}-\varepsilon_{c,\vec{k}+\vec{q}}}, \tag{14}$$

where the indices c, v, k are taken over by the states of conduction, valence and Brillouin zones [19].

The exchange-correlation contribution was:

$$K_{XC}\left(\vec{r},\vec{r}'\right)=\frac{\partial^2 E_{XC}}{\partial\rho(\vec{r})\partial\rho(\vec{r}')}=\frac{dV_{XC}}{d\rho}|_{\rho(\vec{r})}(\vec{r}-\vec{r}') \tag{15}$$

The resulting dielectric matrix is Hermitian, and due to the presence of the center of inversion of the model crystal, is symmetric. Its diagonalization leads to the obtaining of eigenvalues $\in_n^\tau(\vec{q})$ and eigenfunctions $V_n^\tau(\vec{q}+\vec{G})$:

$$\sum_{\vec{G}'}\in^{-1}\left(\vec{q}+\vec{G},\vec{q}+\vec{G}'\right)V_n^\tau\left(\vec{q}+\vec{G}'\right)=\in_n^\tau(\vec{q})V_n^\tau\left(\vec{q}+\vec{G}\right) \tag{16}$$

The vector $\vec{q}$ is in the Brillouin zone; eigenvalues $\in_n^\tau(\vec{q})$ meen the dielectric band structure. Determination of eigenvalues and eigenfunctions are important. They serve to visualize screening in real space, transmit information about the solid state electronic response and allow to adequately take into account the symmetry of the crystal. As in [20, 21], we interpret the obtained eigenvalues of the dielectric matrix as the absorption spectrum. The positions of the optical transitions are determined from the ground-state band structure (Kohn-Sham eigenvalues) by applying the optical selection rules.

Object, results of research and their discussion

For the study of diode and photonic properties of lateral heterostructures based on functionalized graphene depending on the degree of fluorination, a model of a super-lattice was developed. It was a periodic alternation of pure graphene parts (C) and functionalized graphene parts (CH) (Figure 1). The primitive cell of the diamond-type super-lattice has the following parameters: a = 9,96 Å, b = 8,82 Å, c = 5,29 Å and reproduced lateral photonic crystal during translation. The geometric properties of a

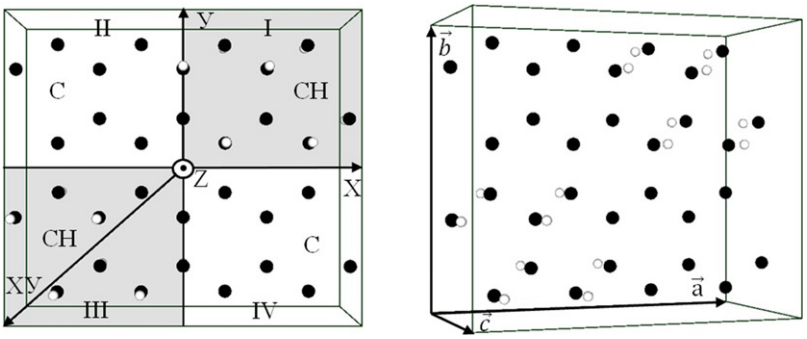

Figure 1. Primitive cell of a super-lattice with an atomic base of lateral C/CH HS – PhC forming unit, top and side views

diamond-type cell are such that it was convenient to use the Cartesian coordinate system (CCS). The size of the primitive cell in the direction Z was chosen so as to avoid the interaction of atomic planes transmitted in this direction. The dimensions of the primitive cell in the directions X and Y were chosen so that during the translation organizes an endless graphene layer. The atoms coordinates in the XY plane of the atomic base were determined as the arithmetic mean of the bond lengths between the carbon atoms of the infinite graphene and graphane sheets. The calculation was performed only for G-points of the Brillouin super-lattice zone. The atomic base contained 48 atoms, of which were 32 C atoms and 16 H atoms.

The modeling process of fluorination was carried out in pairs by replacing the atoms of hydrogen with fluorine atoms. Numerous investigated the following structural configurations: 1) C/CH without fluorine atoms – 0% fluorination; 2) C/CFH (32C + 14H + 2F) with 2 fluorine atoms – 12,5% fluorination; 3) C/CFH (32C + 12H + 4F) with 4 fluorine atoms – 25% fluorination; 4) C/CFH (32C + 10H + 6F) with 6 fluorine atoms – 37,5% fluorination; 5) C/CFH (32C + 8H + 8F) with 8 fluorine atoms – 50% fluorination (Figure 2). The percentage of fluorination was calculated by finding the proportion of fluorine atoms from the total number of hydrogen atoms. In this case, the changes in the electronic and photonic properties of the lateral HS C/CH and C/CFH as PhCs were recorded. Charge values on parts of lateral C/CH and C/CFH HSs depending on the degree of fluorination were calculated (Table 1). They are given in the number of electrons, where in the atomic system of quantum mechanical calculations the charge of an electron is taken equal to one. There was clear charge distribution with different signs on parts of C/CH HS. After fluorination there was a redistribution of charge with increasing charge difference. The highest value of charge redistribution was achieved with 50%-fluorination.

The numerical charge values depending on the degree of fluorination were illustrated by spatial distribution maps of the valence electrons density for C/CH and C/CFH HSs (Figure 3). The process of fluorination increased the covalent C-H bond of functionalized graphene, which manifests itself in increasing the intensity of the valence electrons density along the bonding directions.

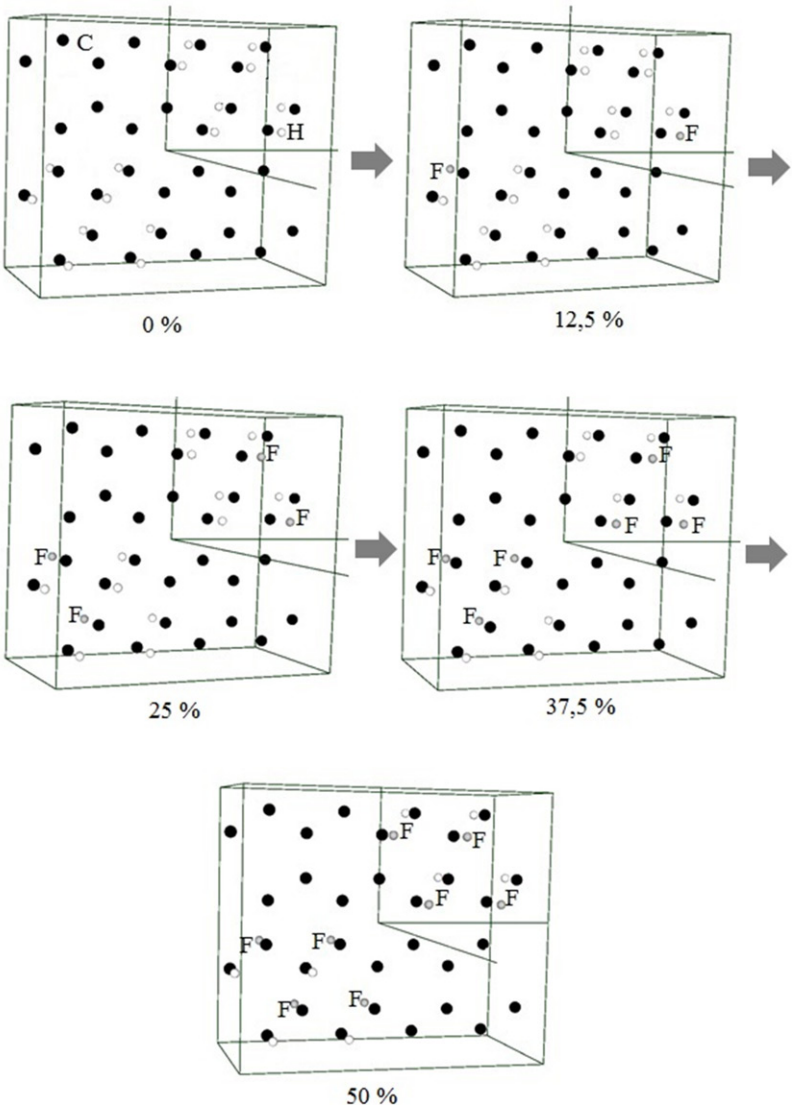

Figure 2. Atomic base of lateral C/CH, C/CFH HSs depending on the degree of fluorination

Change of the band gap width of the lateral C/CH and C/CFH HSs depending on the degree of fluorination was shown in the graph of Figure 4. Numerical values of band gap width of the lateral C/CH and C/CFH HSs were given in Table 2. The non-monotony of the values of the band gap width of C/CH and C/CFH as PhCs was observed with a change in the degree of fluorination. This non-monotony had the oscillation character, in which the HS conductivity varied considerably. Thus, with a certain percentage of fluorination, the HS band gap decreased, and at 37,5%-fluorination it practically disappeared. That is, changing the degree of fluorination on parts of lateral HS C/CFH, can be controlled by their resistive properties.

Table 1. Charge values on parts of lateral C/CH and C/CFH HSs depending on the degree of fluorination

			CCS quarters		
HS (PhC)	% fluorination	Structural configuration	I , III	II, IV	Charge difference
C/CH	0	(32C + 16H)	−35,20	13,40	48,60
C/CFH	12,5	(32C + 14H + 2F)	−39,80	11,65	51,45
	25	(32C + 12H + 4F)	−39,38	10,76	50,14
	37,5	(32C + 10H + 6F)	−42,37	8,76	51,13
	50	(32C + 8H + 8F)	−48,26	6,06	54,32

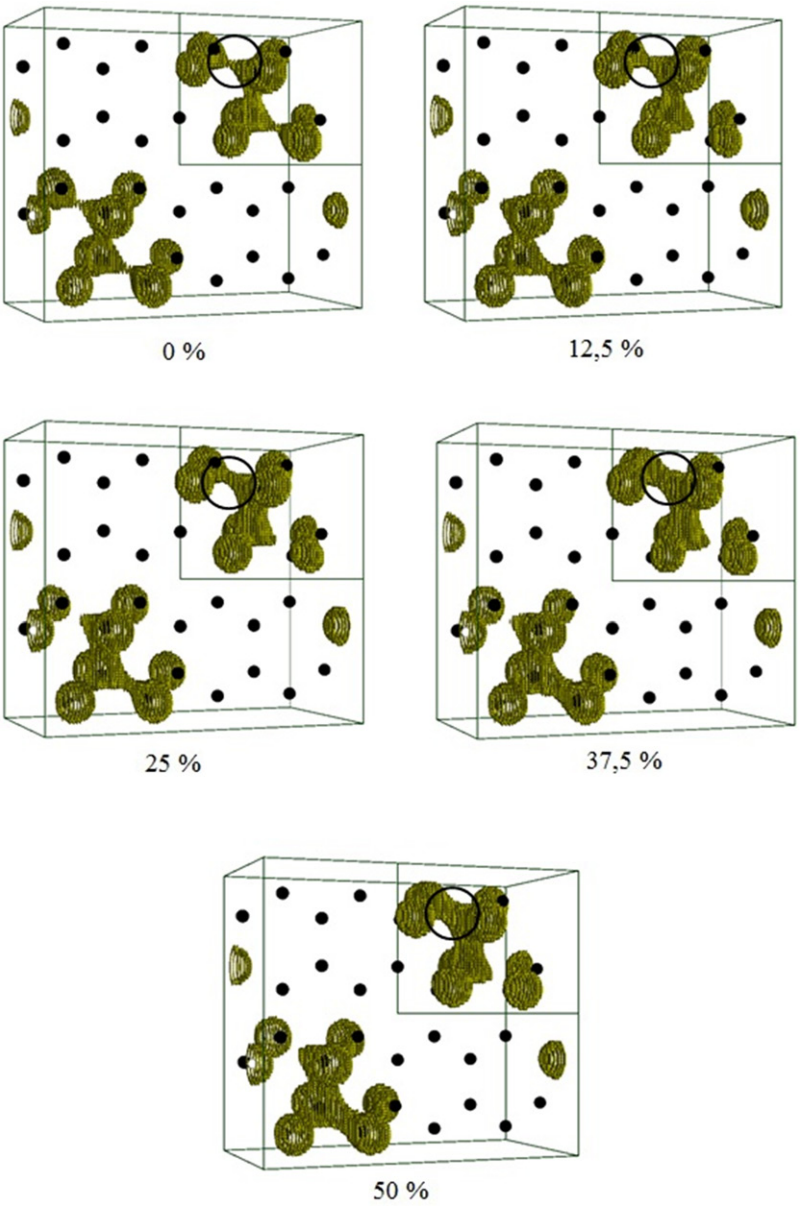

Figure 3. Spatial distribution of valence electrons density for lateral C/CH and C/CFH HSs within the interval of 0.5-0.6 of the maximum value depending on the degree of fluorination

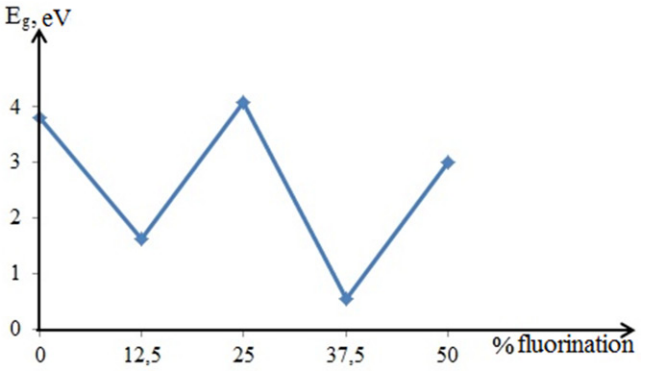

Figure 4. Change of the band gap width of the lateral C/CH and C/CFH HSs depending on the degree of fluorination

Table 2. Band gap width of the lateral C/CH and C/CFH HSs depending on the degree of fluorination

HS (PhC)	% fluorination	Structural configuration	E_g, a.u.	E_g, eV
C/CH	0	(32C + 16H)	0,14	3,81
C/CFH	12,5	(32C + 14H + 2F)	0,06	1,63
	25	(32C + 12H + 4F)	0,15	4,08
	37,5	(32C + 10H + 6F)	0,02	0,54
	50	(32C + 8H + 8F)	0,11	2,99

Table 3. Macroscopic relative permittivity of the lateral C/CH and C/CFH HSs as PhCs in $\vec{E}||\vec{X}$, $\vec{E}||\vec{Y}$, $\vec{E}||[\vec{X}+\vec{Y}]$ directions depending on the degree of fluorination

Direction of the vector of transverse polarization of the electric field of the perturbing electromagnetic wave	% fluorination				
	0	12,5	25	37,5	50
$\vec{E}||\vec{X}$	2,61	0,82	0,89	0,89	0,88
$\vec{E}||\vec{Y}$	1,00	1,00	1,00	1,00	1,00
$\vec{E}||[\vec{X}+\vec{Y}]$	0,96	0,96	0,98	0,97	0,96

The calculated macroscopic relative permittivities of the lateral C/CH and C/CFH HSs as PhCs in the directions of the vector of transverse polarization of the electric field of the perturbing electromagnetic wave depending on the degree of fluorination were given in Table 3. It was seen that the anisotropy of macroscopic dielectric permeability was manifested in all selected directions. The maximum value of the macroscopic relative permittivity was recorded for the $\vec{E}||\vec{X}$ direction of the vector of transverse polarization of the electric field of the perturbing electromagnetic wave with 0%-fluorination. With further fluorination, this value has become much less than unity. That is, the created structure in the direction $\vec{E}||\vec{X}$ has areas that stimulate the passage of electromagnetic wave. In $\vec{E}||\vec{Y}$ and $\vec{E}||[\vec{X}+\vec{Y}]$ directions the values of the macroscopic permittivity were close to one. It coincided with the dielectric vacuum permeability. This value did not involve the refraction of the electromagnetic wave with the distributions along these PhC directions.

Table 4. Wavelengths peaks of the absorption spectrum of the lateral C/CH and C/CFH HSs as PhCs in $\vec{E}||\vec{X}$, $\vec{E}||\vec{Y}$, $\vec{E}||[\vec{X}+\vec{Y}]$ directions depending on the degree of fluorination

HS (PhC)	% fluorination	λ, nm at $\vec{E}||\vec{X}$	λ, nm at $\vec{E}||\vec{Y}$	λ, nm at $\vec{E}||[\vec{X}+\vec{Y}]$
C/CH	0	0,82	258,47	94,82
C/CFH	12,5	19,79	208,57	278,48
	25	136,06	270,27	116,76
	37,5	116,03	148,12	176,72
	50	178,88	165,89	197,61

The own values of the PhC dielectric matrix – wavelengths peaks of the absorption spectrum of the lateral C/CH and C/CFH HSs as PhCs depending on the vector direction and the degree of fluorination were given in Table 4. The own values of the dielectric matrix were listed by comparing them with the electron spectrum at the corresponding wavelengths. Thus, in the direction $\vec{E}||\vec{X}$ with 0%-fluorination (C/CH), the wavelength peak in the absorption spectrum of PhC was 0,82 nm, which corresponds to the area of soft X-ray. For directions $\vec{E}||\vec{Y}$ and $\vec{E}||[\vec{X}+\vec{Y}]$ after fluorination, the peaks of absorption spectrum of the lateral C/CH and C/CFH HSs as PhCs were in the region of ultraviolet radiation.

Absorption spectrum of the lateral C/CH and C/CFH HSs as PhCs depending on the vector direction of transverse polarization of the electric field of the perturbing electromagnetic wave and the degree of fluorination were shown on Figure 5.

Publication was based on the research provided by the grant support of the State Fund for Fundamental Research (project F76/70-2017).

Conclusions

Within the framework of the methods of the electron density functional and the ab initio pseudopotential, the valence electrons density spatial distribution, the densities of electron states, the band gaps, the charges on parts of HSs, the dielectric matrices, and the macroscopic permittivities were obtained. Electronic and photonic properties of the lateral HSs based on functionalized graphene as PhCs depending on the degree of fluorination have been investigated.

It was established that after fluorination there was a redistribution of charge with increasing charge difference. The process of fluorination increased the covalent C-H bond of functionalized graphene, which manifests itself in increasing the intensity of the valence electrons density along the bonding directions.

The values of the band gap width of C/CH and C/CFH as PhCs had the oscillation character, in which the HS conductivity varied considerably. That is, changing the degree of fluorination on parts of lateral HS C/CFH, can be controlled by their resistive properties.

The anisotropy of macroscopic dielectric permeability was manifested in all selected directions. The maximum value was recorded for the $\vec{E}||\vec{X}$ direction of the vector of transverse polarization of the electric field of the perturbing electromagnetic wave with 0%-fluorination. With further fluorination, this value has become much less than unity. That is, the created structure in the direction $\vec{E}||\vec{X}$ has areas that stimulate the passage of electromagnetic wave. In $\vec{E}||\vec{Y}$ and $\vec{E}||[\vec{X}+\vec{Y}]$ directions the values of the

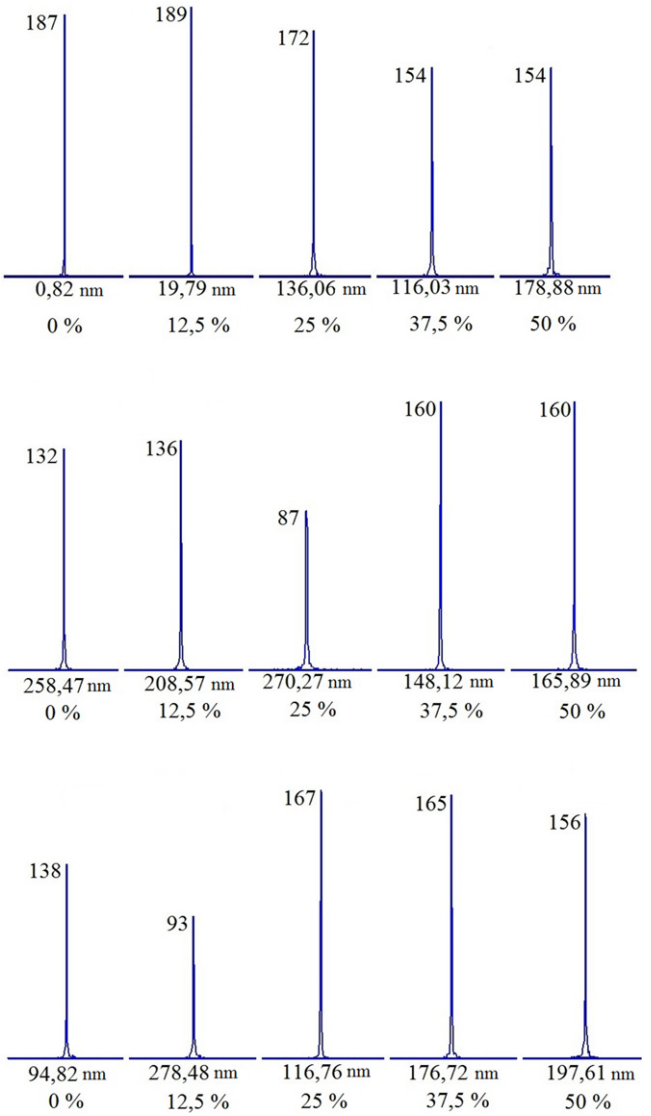

Figure 5. Absorption spectrum of the lateral C/CH and C/CFH HSs as PhCs in $\vec{E}||\vec{X}$, $\vec{E}||\vec{Y}$, $\vec{E}||[\vec{X}+\vec{Y}]$ directions depending on the degree of fluorination

macroscopic permittivity were close to one. It coincided with the dielectric vacuum permeability. This value did not involve the refraction of the electromagnetic wave with the distributions along these PhC directions.

In the direction $\vec{E}||\vec{X}$ with 0%-fluorination, the wavelength peak in the absorption spectrum of PhC was 0,82 nm, which corresponds to the area of soft X-ray. For directions $\vec{E}||\vec{Y}$ and $\vec{E}||[\vec{X}+\vec{Y}]$ after fluorination, the peaks of absorption spectrum of the lateral C/CH and C/CFH HSs as PhCs were in the region of ultraviolet radiation.

References

[1] Solıs-Fernandez P. et al. (2017). *Chem. Soc. Rev*., *46*, 4572–4613.
[2] Balabai R., Solomenko A. (2018). *Appl Nanosci.*
[3] Balabai R.M., Lubenets A.G. (2017). *Journal of Nano- and Electronic Physics*, *9*(5), 05017.
[4] Balabai R.M., Konoval O. A., Solomenko A. G. (2018). *Sensor Electronics and* Microsystem *Technologies*, *15*(3), 58–73.
[5] Berman O., Boyko V., Kezerashvili R. (2018). *Physics Letters A*., *382*, 2075–2080.
[6] Entezar S., Habil M. (2018). *Journal of Magnetism and Magnetic Materials*, *449*, 33–39.
[7] Wang Z., Wang J., Li Z. (2012). *RSC Adv*., *2*, 11681–11686.
[8] Bourlinos A., Bakandritsos A., Liaros N. (2012). *Chem. Phys. Lett*., *543*, 101–105.
[9] Qiu P., Qiu W., Lin Z. (2016). *Nanomaterials*, *69*, 166.
[10] Papadakis I., Bouza Z., Couris S. et. al. (2017). *J. Phys. Chem*., *121*, 22567–22575.
[11] Sofer Z., Simek P., Mazanek V. et. al. (2015). *Chem. Commun*, *51*, 5633–5636.
[12] Ab initio calculation [E-resource] – Mode access to the resource: http://sites.google.com/a/kdpu.edu.ua/calculationphysics.
[13] Hohenberg P., Kohn W. (1964). *Physical review*, *136*(3B), B864.
[14] Kohn W., Sham L. (1965). *Physical review*, *140*(4A), A1133.
[15] Hamann D., Schlüter M., Chiang C. (1979). *Physical Review Letters*, *43*(20), 1494.
[16] Bachelet G., Hamann D., Schlüter M. (1982). *Physical Review B*., *26*(8), 4199.
[17] Ihm J., Zunger A., Cohen M. (1979). *Journal of Physics C: Solid State Physics*, *12*(21), 4409.
[18] Payne M., Teter M., Allan D. (1992). *Reviews of modern physics*, *64*(4), 1045.
[19] Hybertsen M., Louie S. (1987). *Physical Review B*., *35*(11), 5585
[20] Marinopoulos A. G. et al. (2004). Phys. *Rev. B*, *69*, 245419.
[21] Gajdos M. et al. (2006). Phys. *Rev. B*, *73*, 045112.